*B*4-*B*1 phase transition of GaN under isotropic and uniaxial compression

Yansun Yao[1,2,*] and Dennis D. Klug[3]

[1]*Department of Physics and Engineering Physics, University of Saskatchewan, Saskatoon, Saskatchewan, S7N 5E2, Canada*

[2]*Canadian Light Source, Saskatoon, Saskatchewan, S7N 2V3, Canada*

[3]*National Research Council of Canada, Ottawa, K1A 0R6, Canada*

(Received 25 May 2013; revised manuscript received 15 July 2013; published 29 July 2013)

The question raised recently about the mechanisms of the pressure-induced *B*4-*B*1 transition of GaN is investigated using a density functional-based metadynamics method. A homogeneous deformation path through a tetragonal intermediate structure is found to be energetically favorable under hydrostatic pressure conditions. This transition path is initialized by the soft phonon modes that appear along the transverse acoustic branches near the transition point. However, under certain nonhydrostatic pressure conditions an elastic instability replaces the phonon instability to become a dominant mechanism for the structural transformation of GaN. The phase transition would avoid the tetragonal path when a uniaxial stress is applied on the *c* axis but follows a different path through a hexagonal intermediate structure. The selection of the transformation mechanisms, determined by specific stress conditions applied, highlights the important role the competition between phonon and elastic instabilities plays in the reconstructive phase transitions.

DOI: 10.1103/PhysRevB.88.014113 PACS number(s): 81.30.Bx, 62.50.−p, 64.60.My, 71.15.Mb

I. INTRODUCTION

The experimental and theoretical investigations of wide band-gap semiconductor gallium nitride (GaN) have been strongly fostered over recent years due to its rich physical properties and its growing applications in optoelectronic industry.[1–4] Similar to many other group-III nitrides, GaN adopts a hexagonal wurtzite structure (*B*4, space group: $P6_3mc$) under ambient conditions and undergoes a reconstructive phase transition to a cubic rocksalt structure (*B*1, space group: $Fm\text{-}3m$) at high pressure.[5–9] While the critical pressure for this phase transition has been well established, the mechanism that drives the structural transformation has not been fully understood. First-order phase transitions usually have complex mechanisms due to the lack of a common group-subgroup relation between phases.[10] The *B*4-*B*1 transition of GaN is likely to be described by two transformation steps via an intermediate phase. A focus of the current discussions of GaN in literature is on the identification of such a transition pathway that can proceed through the *B*4 to *B*1 phases with the lowest energy cost. At a fixed volume, the wurtzite structure has two structural degrees of freedom, an internal *u* parameter that defines the relative positions of the Ga and N sublattices, and the ratio of the *c* axis to the *a* axis. At ambient conditions, the Ga and N atoms are located in a (nearly) sp^3 tetrahedral network in the *B*4 structure. Saitta and Decremps[11] proposed a tetragonal path for the *B*4-*B*1 transition that is initialized by the closure of the γ angle (120° to 90°) combined with the horizontal movements of the atoms (Fig. 1). A tetragonal intermediate phase would be obtained, which further transforms to a rocksalt structure by a reduction of the c/a ratio (1.633 to 1.414) and an increment of the *u* parameter (0.377 to 0.5). Limpijumnong and Lambrecht[12] suggested an alternative path with a reversed order of the two transformation steps, or a hexagonal path, in which the increment of the *u* parameter proceeds first, instead of the closure of the γ angle; this leads to a hexagonal intermediate (*h*-MgO) structure (Fig. 1). Other transition mechanisms that combine features of both paths have also been proposed.[13]

Concerning the importance of the GaN polymorphs, a large number of studies have been carried out to elucidate the mechanism for this phase transition.[14–18] Recent studies employed a variety of theoretical methods and interatomic potentials that include static modeling,[19] classical and *ab inito* molecular dynamics (MD),[20,21] and transition path samplings.[22] It is generally understood among these studies that the 3*d* orbitals of Ga, conventionally regarded as physically inert, play an important role in selecting the transition path.[14,17] Several MD simulations and transition-path sampling calculations identified the tetragonal path described above as an energetically favorable path for the *B*4-*B*1 transition in GaN under isotropic pressure conditions.[21,22] This is also consistent with the eigenvector analysis of the soft phonon modes that appeared in the *B*4 structure near the transformation pressure.[11] An important aspect of this phase transition remains largely uninvestigated; however, this depends on whether there are significant differences in the phase transition mechanism under uniaxial stress conditions, and whether different intermediate structures, for example, the *h*-MgO structure, may appear by applying certain stresses. Already, recent experiments have revealed that anisotropic stresses may alter the mechanism of the pressure-induced structural transformations in nanocrystalline GaN and boron nitride.[23,24] For this purpose, in the present paper we investigated the mechanistic details of the *B*4-*B*1 transition in GaN where both hydrostatic and nonhydrostatic pressure conditions were considered. An improved version of the metadyanmics method,[25,26] that is, one combined with *ab initio* MD and suited for uniaxial compressions, was employed. Based on MD, this approach takes account of the anharmonic effects that may arise in solids at finite temperatures and is able to characterize the transition pathway from the thermodynamical motions of the atoms without being limited by the constraints of the static modeling.

II. COMPUTATIONAL DETAILS

Structural optimizations, total energies, stress-strain relations, and electronic band structures of GaN were calculated

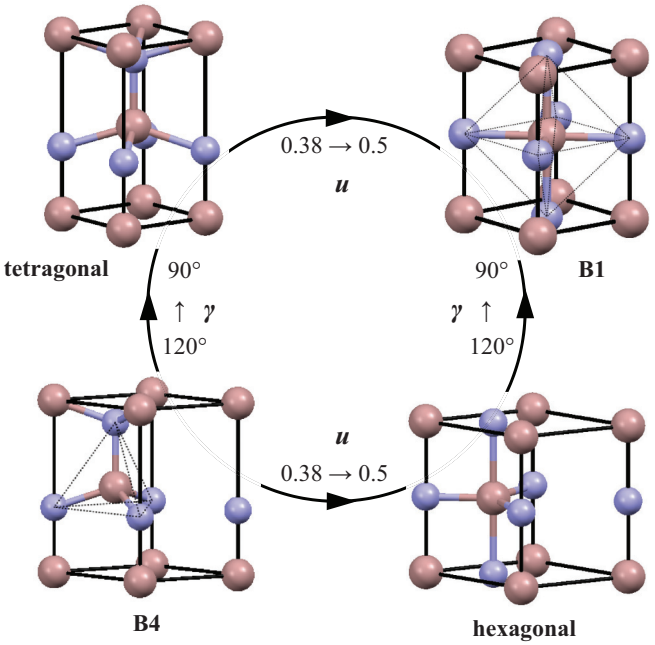

FIG. 1. (Color online) The tetragonal- and hexagonal-transition paths for the pressure-induced $B4$-$B1$ transition in GaN. The two paths both consist of two transformation steps, a closure of the γ angle and an increase of the sublattice spacing u, while the orders of the transformation steps are opposite in the two paths (see text). The Ga and N atoms are represented by tan (larger) and blue (smaller) balls.

using the Vienna *Ab initio* Simulation Package (VASP) program[27] and the projected-augmented wave potentials[28,29] employing the Perdew-Burke-Ernzerhof (PBE) exchange-correlation functional.[30] The Ga and N potentials adopt $3d^{10}4s^24p^1$ and $2s^22p^3$ as valence states, respectively. The plane wave basis set has been carefully checked and found sufficient with an energy cutoff of 980 eV. A $16 \times 16 \times 16$ and $16 \times 16 \times 10$ k-point mesh[31] was used, respectively, to sample the first Brillouin zone (BZ) for the rocksalt and wurtzite structures. Phonons were calculated for the wurtzite structure at room temperature and under strain deformations, employing the self-consistent *ab initio* lattice dynamical (SCAILD) method[32] combined with the VASP program, with a $2 \times 2 \times 3$ supercell (48 atoms) and a $4 \times 4 \times 4$ k-point mesh. To examine the convergence of the supercell size, phonon calculations at selected strains have been repeated using a larger $3 \times 3 \times 3$ supercell (108 atoms) and a $4 \times 4 \times 4$ k-point mesh. It was found from this test that the calculated phonon frequencies are converged within 0.1 THz ($\sim$3.34 cm^{-1}).

The metadynamics method designed for the simulations of solid-solid phase transitions[33] was employed and combined with the VASP program and a recent modification for the simulation[25,26] of nonhydrostatic pressure conditions, which uses the same PBE potentials described above. The new formulation explicitly treats the uniaxial pressures by decomposing the energy derivatives with respect to simulation cell matrix into anisotropic and hydrostatic components and utilizes them as the driving force for structural evolution. The scanning of energy landscape usually starts with a local energy well with the shape of the well roughly sketched by Hessian matrix and proceeds by gradually filling up the well with Gaussian functions. Once the initial well is filled, the system will migrate to other wells; this corresponds to structural changes. It should be noted that the density functional theory (DFT)-based methods based on modified versions of quasiharmonic approximation have been applied to investigate complex phase transitions in solid materials and demonstrated successful in reproducing the experimental observables.[34] The metadynamics method is complimentary to these methods in terms of an accurate prediction of the transition pressure, and, in addition, the former is able to reveal detailed microscopic mechanism for the phase transitions under general temperature-pressure conditions. The supercells employed in the metadynamics calculations contained 64 atoms, and a dense $3 \times 3 \times 3$ k-point mesh was used to ensure a convergence of the total energy to a few meV per atom. Each metastep consists of a first-principles MD simulation employing a canonical ensemble (NVT), with 400 time steps for a total simulation time of 0.8 ps. Gaussian width and height parameters were chosen following the guidelines, summarized recently in Ref. 35. Elastic instabilities were investigated through evaluation of the Born stability conditions obtained from calculations of the elastic constants for a uniaxially strained wurtzite structure.[36–40]

III. RESULTS AND DISCUSSION

A. Enthalpies

The calculated enthalpies $H = E + PV$ as functions of pressures for the wurtzite and rocksalt structures of GaN are compared in Fig. 2. The predicted critical pressure for the $B4$-$B1$ transition is near 44.8 GPa, which agrees well with the previously calculated values of 42.9 GPa–51.8 GPa.[11,15,17,19,41] The present calculation also compares well with the measured phase-transition pressures that range from 37 GPa to 53.6 GPa, within the error bars associated with a large hysteresis cycle.[5–9] The energy orders of the $B4$ and $B1$ structures at finite temperatures may be refined by their Gibbs-free energies. The Gibbs-free energies in solids are usually obtained

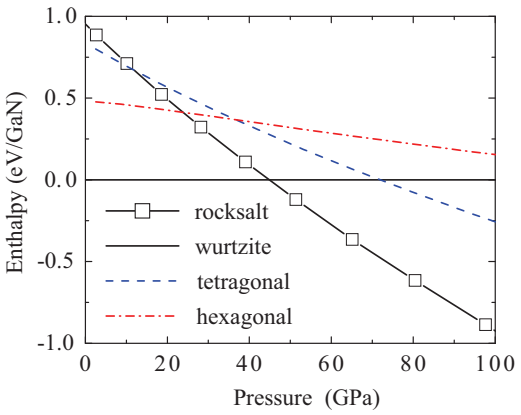

FIG. 2. (Color online) Calculated enthalpies per GaN unit for the $B4$, $B1$, tetragonal-, and hexagonal-intermediate structures in the pressure range 0–100 GPa. The enthalpies of the $B4$ structure are taken as the reference.

from quasiharmonic approximations.[34,42] In the present case, however, the $B4$-$B1$ transition is initialized by the soft phonon modes that appear along the transverse acoustic branches near the transition point.[11] The soft phonon modes make a direct evaluation of the Gibbs-free energy difficult, but the stabilities of the $B4$ structure at finite temperature can be inferred from the metadynamics simulations (see later). Notably, if we use the same PBE functional but eliminate the $3d$ electrons from Ga valence states, the calculated critical pressure for the $B4$-$B1$ transition will be reduced substantially to 31.1 GPa. A similar trend has also been observed in previous studies,[17] which, in a way, demonstrates the important role that the $3d$ orbitals play in this phase transition.

One way to look at this orbital-based change of the critical pressure is from the nearest-neighbor electrostatic interactions. The energy level of the $2s$ state in nitrogen atom is very close to that of the $3d$ state in the gallium atom, i.e., their energy difference is less than 1.6 eV.[14] In both $B4$ and $B1$ structures, since the Ga and N are located at each other's nearest-neighbor site, resonance effects will arise between the Ga $3d$ and N $2s$ states. The nearest-neighbor closed-shell repulsions that arise between core states or between core and valence states are also strengthened. In a reduced volume, these effects are enhanced by the increased orbital overlap. The Ga $3d$ orbitals can no longer be assumed to be physically inert anymore when the system is under sufficient compression. At this point, neglecting the Ga $3d$ states in the valences will result in an undercounting of closed-shell repulsion contributions, therefore, an underestimate of the total energy. Compared with the $B4$ structure, the $B1$ structure has an increased Ga/N coordination and, therefore, stronger overall closed-shell repulsions. Thus, the $B1$ structure would suffer more energy loss than the $B4$ structure at high pressure if the Ga $3d$ electrons are not included in the calculation; this is reflected in a reduction of the phase-transition pressure. The second nearest-neighbor interactions, i.e., direct Ga-Ga repulsions, are much weaker and, therefore, contribute insignificantly to the phase-transition pressure.

The enthalpies of the tetragonal- and hexagonal-intermediate structures were calculated and compared with the enthalpies of the $B4$ and $B1$ structures (Fig. 2). These intermediate phases are shown as saddle points in the potential energy surface,[43] which, if fully relaxed, will yield either the $B4$ or the $B1$ structure. Thus, the enthalpies of the intermediate structures have to be calculated with constraints by fixing one or more structural degrees of freedom.[44] In order to maintain a basic symmetry of a transition path, the space group was chosen as a constraint for all intermediate structures. Along the tetragonal and hexagonal paths, the intermediate structures are fixed in the $I4mm$ and $P6_3/mmc$ space groups, respectively. At each pressure, the cell parameters and Wyckoff positions are relaxed within the fixed space group with respect to the trace of stress tensors. The enthalpies calculated in this manner provide an upper-bound estimate of the activation barrier along a phase-transition path. For the present case, the hexagonal intermediate structure is more energetically favorable than the tetragonal one only in a low-pressure range where the $B4$-$B1$ phase transition is prohibited. The thermodynamic stabilities of the two intermediate structures exchange near 37 GPa. At the phase-transition pressure, i.e., 44.8 GPa, the tetragonal-intermediate structure is already more stable than the hexagonal one and, therefore, represents a lower energy transition state.

B. Stress-strain relations

We investigated the phonon eigenmodes and ideal strengths of the $B4$ structure under certain strain deformations. We also investigated the Born stability conditions as obtained from calculations of the elastic constants at the pressure corresponding to the $B4$-$B1$ phase transition. The five independent elastic constants of the $B4$ structure were also evaluated at ambient pressure for comparison with the literature. The calculated ambient pressure elastic constants are $C_{11} = 322$ GPa, $C_{12} = 115$ GPa, $C_{13} = 83$ GPa, and $C_{44} = 92.43$ GPa, in very good agreement with the values tabulated in Ref. 45. The phonon eigenmodes characterize the dynamical instability of a material, while the stability requires that the frequencies be real for all wavevectors in the BZ. The ideal strength of a material is a critical stress along a homogenous strain direction where the crystal becomes elastically unstable. In some respects, an elastic instability may be considered as a phonon instability that appears at the BZ center with vanishing wave vectors. This ideal strength is an important measure for material failure under uniaxial strains.

For the $B4$-$B1$ phase transition of GaN, the uniaxial compression along the c axis is of particular relevance. A current hypothesis is that under this deformation, the $B4$-$B1$ phase transition will proceed through a hexagonal path, even though this path is not energetically favorable under the hydrostatic pressure conditions.[12] To this end, we calculated the stress-strain curve for the uniaxial compression of the $B4$ structure at the phase-transition pressure, i.e., 44.8 GPa, using a quasistatic method[46,47] [Fig. 3(a)]. In this approach, the unit cell of the $B4$ structure is incrementally deformed along the c axis, with the uniaxial strain defined as $\varepsilon_{33} = (c - c_0)/c_0$, where c_0 represents the lattice constant optimized at 44.8 GPa. At each deformation step, the structure is relaxed until the stress tensors orthogonal to the applied strain reaches 44.8 GPa, and the Hellmann-Feynman forces on each atom reduces to below 0.003 eV/Å while maintaining the strain condition. The solid symbol in Fig. 3(a) indicates the onset of the strain-induced phonon instability, which occurs when the c axis is shortened to ~80% of the original value ($\varepsilon_{33} = -0.19$). A low-lying transverse acoustic branch is substantially softened at this point, and several imaginary modes appear around the Γ and M points [Fig. 3(b)]. The elastic instability, in comparison to the phonon instability, occurs much earlier at $\varepsilon_{33} = -0.08$, as shown by the calculated ideal strength in the the stress-strain curve. We also examined the five independent elastic constants of the $B4$ structure as a function of uniaxial strain by application of the Born stability conditions following the method described in Ref. 37. From the evaluation of the Born stability condition $(C_{11} + C_{22}) \times C_{33} - 2 \times C_{13}^2 > 0$, we obtained the same elastic instability at $\varepsilon_{33} = -0.08$ for the uniaxially strained $B4$ structure [Fig. 3(c)]. The remaining Born stability conditions for a hexagonal crystal, $C_{11} - |C_{12}| > 0$, $C_{11} - C_{12} > 0$, and $C_{44} > 0$ are obeyed in

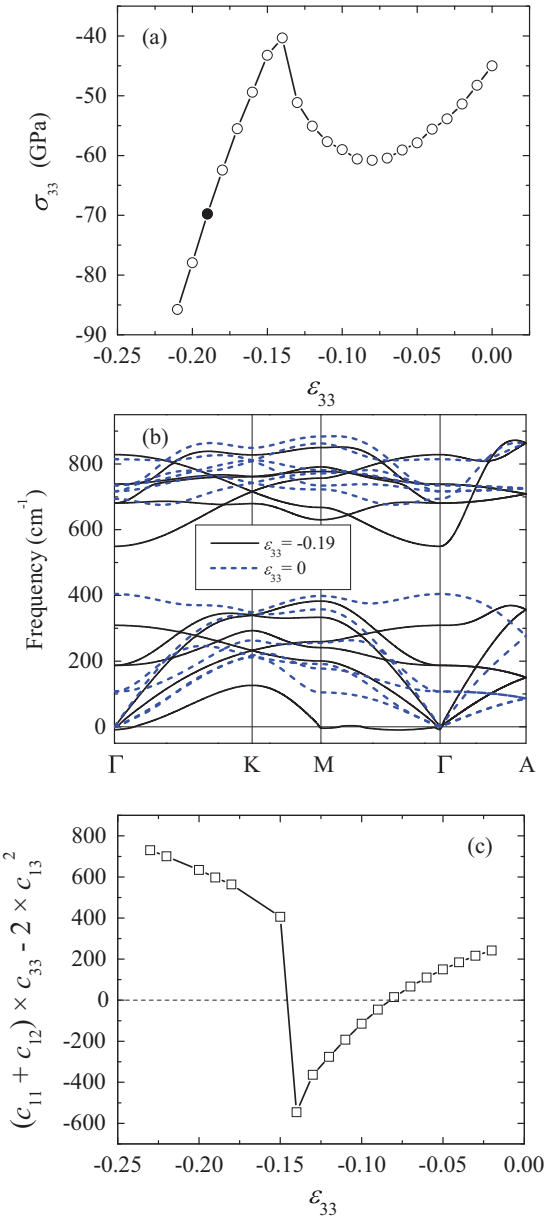

FIG. 3. (Color online) (a) Calculated stress-strain relation of the $B4$ structure under a uniaxial compression along the c axis. The solid circle indicates the appearance of the phonon instability determined at room temperature using the SCAILD method. (b) Calculated SCAILD phonon-band structures of the $B4$ structure at $\varepsilon_{33} = 0$ and $\varepsilon_{33} = -0.19$. (c) Calculated Born stability condition $(C_{11} + C_{22}) \times C_{33} - 2 \times C_{13}^2 > 0$ under a uniaxial compression along the c axis as a function of the strain parameter ε_{33}.

this region for ε_{33}. Significantly, the results in Figs. 3(a) and 3(c) indicate that under a uniaxial compression, the elastic instability becomes the dominant mechanism for the structural transformation of GaN. It is interesting that a similar scenario, i.e., competitions between phonon and elastic instabilities, has also been observed in Al.[46,47]

Under the critical strain condition, the magnitude of the σ_{33} stress tenor is increased to about 66.82 GPa, nearly 1.5 times larger than the stress tensors along the orthogonal directions. The peak σ_{33} corresponds to the ideal strength for this uniaxial strain, and it sets an upper bound of the anisotropic pressure load that the $B4$ structure can attain before the structure breaks down. Upon further increasing the strain, the magnitude of the σ_{33} starts to decrease in the $B4$ structure, indicating the onset of a material failure. Once the strain reaches -0.14, where the c axis shrinks to 86%, the $B4$ structure cannot be retained without a phase transition. We found that the $B4$ structure spontaneously transforms to a hexagonal intermediate state, similar to the state illustrated in Fig. 1, once this strain condition is applied. Compared with its tetragonal counterpart, the hexagonal intermediate structure can conveniently adopt a reduced c/a ratio induced by the uniaxial stress. After this phase transition, the Born stability condition $(C_{11} + C_{22}) \times C_{33} - 2 \times C_{13}^2 > 0$ is obeyed, and the magnitude of the stress tensor increases again [Fig. 3(c)]. This observation, although confined by the use of a static model, supports the suggestion that the $B4$-$B1$ phase transition of GaN would proceed via a hexagonal intermediate structure under uniaxial pressure conditions. A more direct investigation of this phase transition is carried out by a survey of the free-energy landscape using the density functional metadynamics simulations that couple all thermodynamic variables and motions of atoms (see below).

C. Phase transitions

The stress-strain relations and phonons calculated above provide an upper-bound estimate of the potential energy surface in GaN under uniaxial strains. To directly examine the free-energy surface that defines the stability regions for a structure in the phase diagram, metadynamics simulations are employed and combined with first-principles MD calculations to study the phase transitions of GaN. A goal is to search for low-energy cost pathways leading from the initial $B4$ structure to the final $B1$ structure, which may proceed via different intermediate structures under different stress conditions. The present metadynamics implementation employs scaled cell vectors of the simulation cell $\mathbf{h}$ as collective variables, defined as an upper triangular matrix with a six-component vector $(h_{11}, h_{22}, h_{33}, h_{12}, h_{13}, h_{23})$. Six dominant modes of cell deformations are derived from the elastic response matrix, also known as the Hessian matrix, defined as the second derivative of the Gibbs-free energy G with respect to the cell variations. The eigenvectors of the Hessian matrix projected on the cell vectors describe six elastic modes. The driving force that guides the evolution of the simulation cell is the derivative of the G,

$$-\frac{\partial G}{\partial h_{ij}} = V[\mathbf{h}^{-1}(\mathbf{p} - P)]_{ji} - V_0\left[\mathbf{h}_0^{-1}\Sigma\mathbf{h}_0^{T-1}\mathbf{h}^T\right]_{ji}. \quad (1)$$

Here the $\mathbf{p}$ is the internal stress tensor obtained from the MD trajectories after equilibration of the system, and $\mathbf{h}_0$ is a reference value of $\mathbf{h}$. To adopt a uniaxial strain condition, the external stress tensor is decomposed into hydrostatic (P) and anisotropic (Σ) components, i.e., $\mathbf{P}_{\text{ext}} = \Sigma + P$ and $P = \text{Tr}(\mathbf{P}_{\text{ext}})/3$ (see Ref. 48). In the simulation that follows, the magnitude of the Σ is set as 10% of the P, i.e., $\Sigma_{33} = -2\Sigma_{11} = -2\Sigma_{22} = 6.67\%\ P$. We have chosen a moderate value for the Σ here to ensure that the metadynamics simulation starts within the elastic stability limit. A prerequisite for the

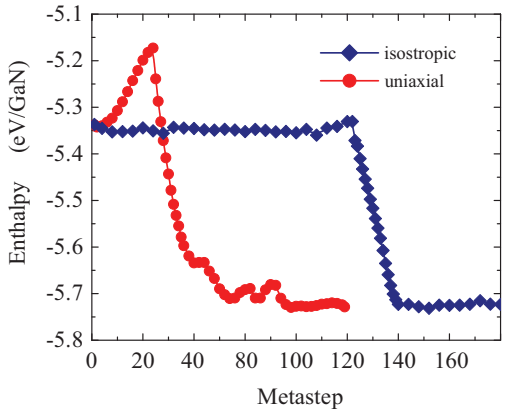

FIG. 4. (Color online) The enthalpies derived from the metadynamics trajectories of GaN under isotropic and uniaxial pressure conditions starting from the $B4$ structure at 300 K and 50 GPa.

metadynamics simulation implemented in the current form is that the structural evolution needs to begin from a stable configuration (a local or global energy minimum).

The metadynamics simulations starting from the initial $B4$ structure revealed distinctly different behavior at $P = 50$ GPa under isotropic and uniaxial pressure conditions (Fig. 4). Under hydrostatic $\mathbf{P}_{\text{ext}}$, the structural evolution initially proceeds steadily without notable enthalpy changes until metastep 88. After overcoming a small enthalpy barrier ($\sim$0.03 eV/GaN) by metastep 102, the configuration proceeds quickly downhill to a $B1$ structure. The phase transition completes at metastep 122. Under nonhydrostatic $\mathbf{P}_{\text{ext}}$, the structural transformation immediately starts at the beginning, and this brings the enthalpy to a steep barrier ($\sim$0.17 eV/GaN). The configuration then proceeds to a $B1$ structure through steps and completes the $B4$-$B1$ phase transition at metastep 55. The anisotropic stress Σ was turned off at metastep 72 to allow the phase transition to settle into an unstrained final structure. The microscopic mechanisms are characterized for both phase transitions. Figure 5(a) shows the evolutions of the six vectors of the simulation cell under hydrostatic $\mathbf{P}_{\text{ext}}$. In this case, the h_{11}, h_{22}, h_{33}, and h_{12} modes are activated during the $B4$-$B1$ phase transition, while the other two modes remain inactive. The eigenvalues of all the excited modes become negative, suggesting a reduction of the volume after this phase transition. Notably, the combination of the four active modes reveals a tetragonal path, as demonstrated in Fig. 5(b) by the structural evolution at different stages of the transition. The h_{12} shearing mode distorts the (001) planes, which can therefore adopt the $B1$ face planes after a slight rotation around the c axis. Simultaneously, the size of the (001) planes also reduces by a shortening of the h_{11} and h_{22} to accommodate the increased packing density. A reduction in the h_{33} indicates the change of the c/a ratio from $\sim$1.633 to $\sim$1.414. The internal u parameter that measures the spacing between the Ga and N sublattices is evolved progressively through the MD simulations made at each metastep. Under nonhydrostatic $\mathbf{P}_{\text{ext}}$, the evolution of the simulation cell follows a completely different path [Fig. 6(a)]. The first 24 metasteps feature an enthalpy change in which only the h_{11} and h_{33} modes are activated. Significantly, these two modes, followed by an increment of the u parameter, lead

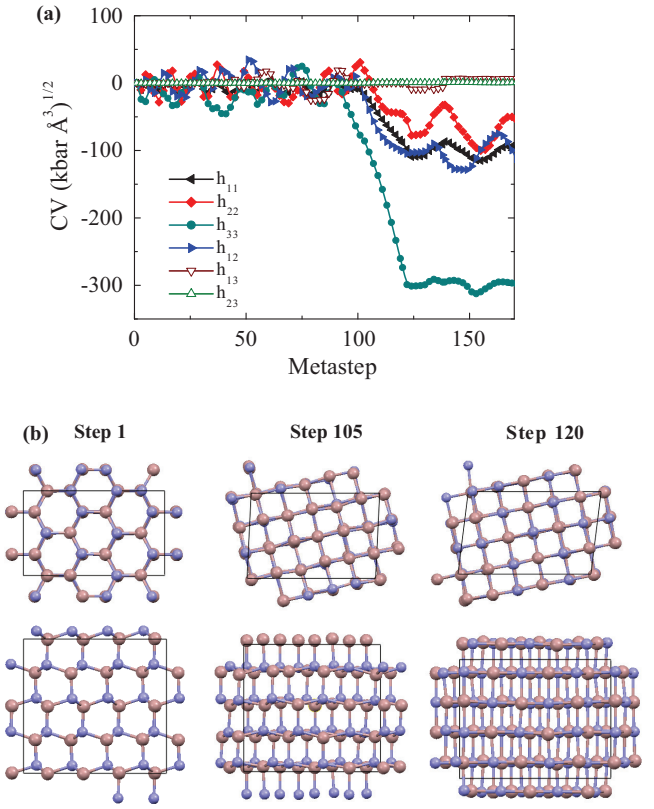

FIG. 5. (Color online) (a) Evolution of the six vectors of the simulation cell matrix indicating a phase transition initialized at metastep 88 from the metadynamics simulation at 300 K and under hydrostatic pressure of 50 GPa. (b) Instantaneous simulation cell viewed along the [001] (upper) and [100] (lower) directions at selected metasteps showing a direct $B4$-$B1$ phase transition along the tetragonal path. The Ga and N atoms are represented by tan (larger) and blue (smaller) balls. The average Ga-N bond lengths in the three metasteps are 1.83 Å, 1.94 Å, and 2.05 Å, respectively.

the structural transformation toward a hexagonal intermediate structure [metastep 24, Fig. 6(b)]. Since the h_{12} mode remains inactive, the (001) planes maintain a basic hexagonal shape, while the h_{11} increment only slightly modifies the in-plane atomic arrangements. The initial reduction of the h_{33} clearly results from a greater pressure load on the c axis, which progressively pushes the configuration beyond the elastic stability limit. After metastep 24, the h_{12} and h_{22} modes are activated and, in some respects, are very similar to the first transition stage under the hydrostatic $\mathbf{P}_{\text{ext}}$ restructuring of the (001) planes into the $B1$ face planes.

Different transition mechanisms revealed under isotropic and uniaxial stress conditions highlight the competitions between the phonon and elastic instabilities. In a theoretical study, Saitta and Decremps suggested that the tetragonal path favored under hydrostatic pressure is facilitated by the soft phonon modes on the transverse acoustic (TA) branches along the $\Gamma \rightarrow A$ direction, which corresponds to a closure of the γ angle.[11] This suggestion is supported by an experimental study of this phase transition[49] using Raman scattering and optical absorption spectroscopy, where no evidence of the hexagonal intermediate structure was found under quasihydrostatic pressure conditions (silicone oil was used as the

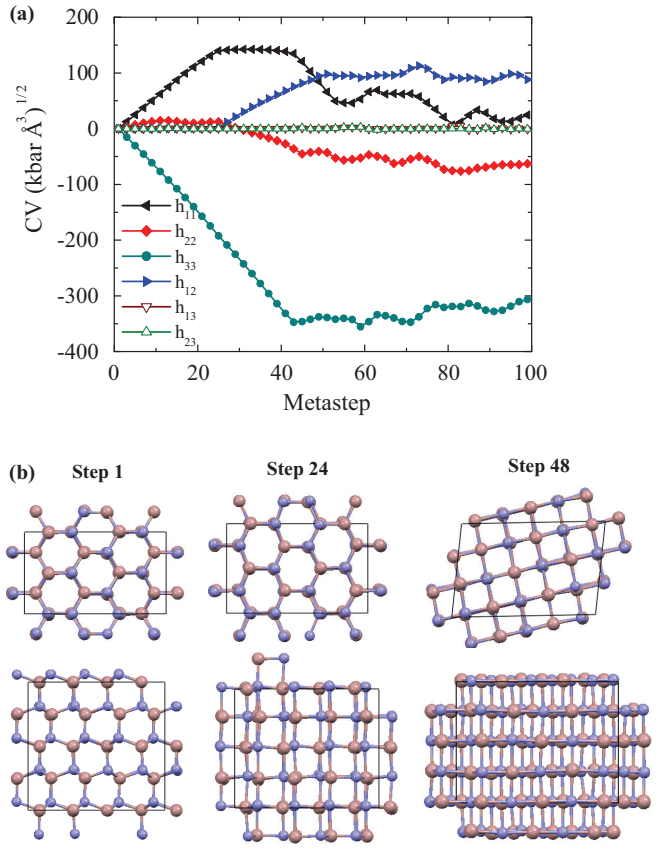

FIG. 6. (Color online) (a) Evolution of the six vectors of the simulation cell matrix showing an immediate structure change under nonhydrostatic pressure (50 GPa). (b) Instantaneous simulation cell viewed along the [001] (upper) and [100] (lower) directions at selected metasteps showing a direct $B4$-$B1$ phase transition along the hexagonal path. The Ga and N atoms are represented by tan (larger) and blue (smaller) balls. The average Ga-N bond lengths in the three metasteps are 1.83 Å, 1.85 Å, and 2.05 Å, respectively.

pressure-transmitting medium). Under uniaxial stresses, the elastic instability, however, may replace the phonon instability to become the dominant mechanism, and this would change the phase-transition route. Using the metadynamics simulation, we predicted that a hexagonal path can also appear for the same phase transition if a uniaxial compression is applied, even though this path is associated with a larger energy barrier. This prediction may be verified experimentally if the appropriate pressure conditions can be used.

To obtain a general view of this phase transition, we calculated the static energy landscape of GaN at 50 GPa, using the γ angle and the u parameter as variables (Fig. 7). At this pressure, the $B4$ (120°, 0.38) and $B1$ (90°, 0.5) structures are identified as a local and global energy minima, respectively. It is interesting that near both minima, the energy surface is much flatter along the variations of the γ angle than along the variations of the u parameter. This provides a qualitative explanation, from the view of energetics, of why the tetragonal path is intrinsically more favored than the hexagonal path. The two transition trajectories derived from the metadynamics simulations are mapped into the energy landscape by dashed lines with filled squares (isotropic compression) and spheres

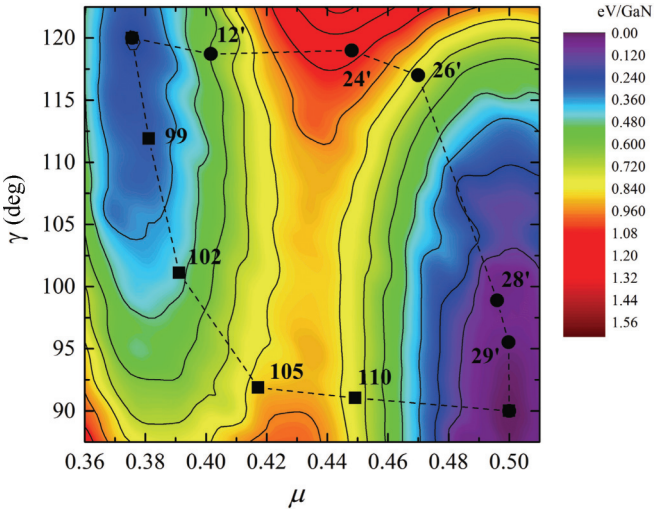

FIG. 7. (Color online) Contour plot of the minimized enthalpies of GaN as a function of the γ angle and the sublattice spacing u at 50 GPa. The enthalpy of the $B1$ structure is taken as a reference. The average (γ, u) derived from the metadynamics trajectories are represented by filled squares (isotropic compression) and filled spheres (uniaxial compression). Numbers next to the symbols indicate the metastep numbers. The dashed lines are given as guides to the eye. For the enthalpy calculation, the γ and u were kept fixed at each point, while all other degrees of freedom of the structure were optimized, with respect to the trace of stress tensors at 50 GPa.

(uniaxial compression). Under hydrostatic pressure, the configuration initially moves downward of the shallow-energy valley by closing the γ angle. At metastep 105, the γ angle is already reduced to below 92°, while the u parameter slightly increases to above 0.41. This may be considered as a configuration closest to the tetragonal intermediate structure. Afterward, the configuration proceeds to the $B1$ structure by mainly increasing the u parameter. Under nonhydrostatic pressure, the increment of the u parameter occurs first, prior to the closure of the γ angle; this induces a large energy barrier in the first two dozen metasteps. By metastep 26, the u parameter is increased to 0.47, while the γ angle slightly reduced to 117°. This may be considered as a configuration closest to the hexagonal intermediate structure. After metastep 26, the configuration descends downhill through the energy valley mainly by reducing the γ angle. Clearly, both phase transitions follow a distinct two-step path that is essentially the tetragonal path or hexagonal path described in Fig. 1.

Both tetragonal and hexagonal intermediate structures have a fivefold coordination (Fig. 1), which is consistent with the four- to six-coordination change for the $B4$-$B1$ transition. The electronic structures, however, are different in these two structures. The $B4$ structure has a direct band gap of 2.6 eV (DFT value) at the phase-transition pressure [Fig. 8(a)]. In the hexagonal-intermediate structure, the band-gap magnitude is almost unchanged from the value in the $B4$ structure, but the gap develops into a pseudodirect one along the $\Gamma \rightarrow H$ direction [Fig. 8(b)]. A similar direct–pseudodirect transition has also been predicted in other Ga-based semiconductors.[50] The tetragonal-intermediate structure, on the other hand, contains an indirect band gap with a largely reduced magnitude (~0.9 eV) [Fig. 8(c)]. It is interesting that the isotropic

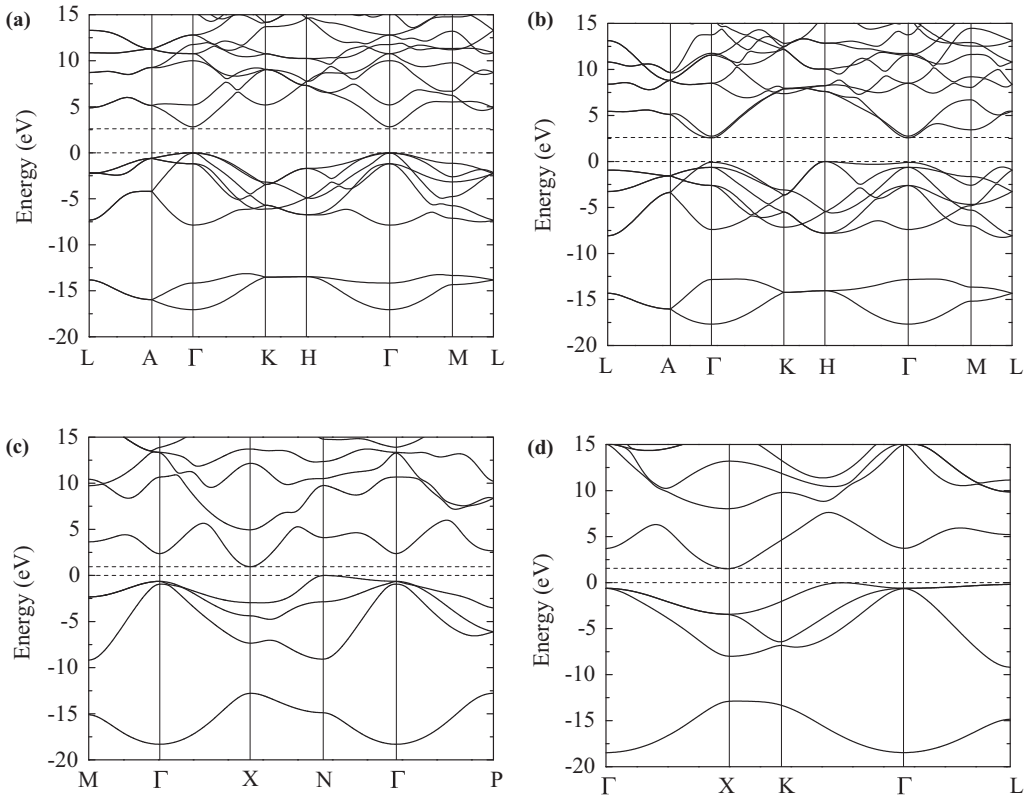

FIG. 8. Calculated electronic band structures at 50 GPa for (a) the $B4$ structure, (b) the hexagonal-intermediate structure, (c) the tetragonal-intermediate structure, and (d) the $B1$ structure. Dashed lines denote the energies of the valence and conduction bands.

compression tends to decrease the band gap and also makes it indirect, while the uniaxial compression tends to maintain a direct band gap. Beyond the tetragonal intermediate structure towards the $B1$ structure, the band gap increases again but stays indirect [Fig. 8(d)]. It is worth mentioning at this point that in a previous experiment,[6] the GaN crystal turned black, and the Raman signal was lost at the onset of the $B4$-$B1$ transition, which may be related to the change of the band gap during the phase transition.

IV. SUMMARY

The present study provides a theoretical investigation of the pressure-induced $B4$-$B1$ transition in GaN. Static enthalpy calculations show that the $B1$ structure would become more stable than the $B4$ structure near 44.8 GPa. This agrees well with the previously measured and calculated critical pressures for this phase transition. The $B4$-$B1$ transition of GaN may be described by two major deformation steps: (1) a closure of the hexagonal angle γ and (2) an increment of the spacing u between Ga and N sublattices. The sequence of these two steps determines the detailed transformation path and intermediate structures. Under hydrostatic pressure conditions, a tetragonal path in which the γ changes ahead of the u, was found to be energetically more favorable than a hexagonal path with the reversed sequence of steps. Near the phase-transition point, calculated stress-strain relations and phonon eigenmodes revealed a competition between elastic instability and dynamical instability, which represent two different transformation mechanisms. Using an improved version of the metadyanmics methods, the $B4$-$B1$ transition of GaN has been directly simulated under both isotropic and uniaxial pressure conditions. Under an isotropic compression, the phase transition proceeds through a tetragonal path facilitated by unstable phonon modes on the TA branches. Under the uniaxial compression, in contrast, the elastic instability becomes a dominant mechanism, which alters the phase transition path to a hexagonal one. Following the tetragonal path, a direct-to-indirect gap transition is predicted to occur, along with a large decrease of the band gap. This prediction may therefore be relevant to the observation in previous experiments where the Raman signal disappeared and the GaN sample turned black at the onset of the phase transition. The present study provides new insights that help to reconcile the recent experimental and theoretical controversy regarding the mechanism of the $B4$-$B1$ transition in GaN.

ACKNOWLEDGMENTS

Y. Yao gratefully acknowledges the Information and Communications Technology group at the University of Saskatchewan for providing computing resource, the Socrates cluster, which is part of the High Performance Computing Training and Research Facilities at the University of Saskatchewan. Part of the calculations has been performed by the use of computing resources provided by WestGrid, Compute Canada, and National Research Council of Canada. This project was supported by a Natural Sciences and Engineering Research Council of Canada (NSERC) Discovery Grant.

*Corresponding author: yansun.yao@usask.ca

[1] S. Nakamura and G. Fasol, *The Blue Laser Diode* (Springer Verlag, Berlin, 1997).
[2] F. A. Ponce and D. P. Bour, Nature **386**, 351 (1997).
[3] A. Rubio, J. L. Corkill, M. L. Cohen, E. L. Shirley, and S. G. Louie, Phys. Rev. B **48**, 11810 (1993).
[4] J. W. Orton and C. T. Foxon, Rep. Prog. Phys. **61**, 1 (1998).
[5] A. Muñoz and K. Kunc, Phys. Rev. B **44**, 10372 (1991).
[6] P. Perlin, C. Jauberthie-Carillon, J. P. Itie, A. SanMiguel, I. Grzegory, and A. Polian, Phys. Rev. B **45**, 83 (1992).
[7] H. Xia, Q. Xia, and A. L. Ruoff, Phys. Rev. B **47**, 12925 (1993).
[8] M. Ueno, M. Yoshida, A. Onodera, O. Shimomura, and K. Takemura, Phys. Rev. B **49**, 14 (1994).
[9] S. Uehara, T. Masamoto, A. Onodera, M. Ueno, O. Shimomura, and K. Takemura, J. Phys. Chem. Solids **58**, 2093 (1997).
[10] A. Mujica, A. Rubio, A. Munoz, and R. J. Needs, Rev. Mod. Phys. **75**, 863 (2003).
[11] A. M. Saitta and F. Decremps, Phys. Rev. B **70**, 035214 (2004).
[12] S. Limpijumnong and W. R. L. Lambrecht, Phys. Rev. Lett. **86**, 91 (2001).
[13] H. Sowa, Acta Crystallogr. Sect. A **57**, 176 (2001).
[14] V. Fiorentini, M. Methfessel, and M. Scheffler, Phys. Rev. B **47**, 13353 (1993).
[15] N. E. Christensen and I. Gorczyca, Phys. Rev. B **50**, 4397 (1994).
[16] K. Parlinski and Y. Kawazoe, Phys. Rev. B **60**, 15511 (1999).
[17] J. Serrano, A. Rubio, E. Hernández, A. Muñoz, and A. Mujica, Phys. Rev. B **62**, 16612 (2000).
[18] L. Qin, Y. Duan, H. Shi, L. Shi, and G. Tang, J. Phys.: Condens. Matter **25**, 045801 (2013).
[19] J. Cai and N. Chen, Phys. Rev. B **75**, 134109 (2007).
[20] H. Xiao, X. Jiang, G. Duan, F. Gao, X. Zu, and W. J. Weber, Comput. Mater. Sci. **48**, 768 (2010).
[21] H. Xiao, F. Gao, L. Wang, X. Zu, Y. Zhang, and W. J. Weber, Appl. Phys. Lett. **92**, 241909 (2008).
[22] S. E. Boulfelfel, D. Zahn, Yu. Grin, and S. Leoni, Phys. Rev. Lett. **99**, 125505 (2007).
[23] Z. Dong and Y. Song, Appl. Phys. Lett. **96**, 151903 (2010).
[24] C. Ji, V. I. Levitas, H. Zhu, J. Chaudhuri, A. Maranthe, and Y. Ma, Proc. Natl. Acad. Sci. USA **109**, 19108 (2012).
[25] D. Donadio, R. Martoňák, P. Raiteri, and M. Parrinello, Phys. Rev. Lett. **100**, 165502 (2008).
[26] Y. Yao and D. D. Klug, Phys. Rev. B **86**, 064107 (2012).
[27] G. Kresse and J. Hafner, Phys. Rev. B **47**, 558 (1993).
[28] P. E. Blöchl, Phys. Rev. B **50**, 17953 (1994).
[29] G. Kresse and D. Joubert, Phys. Rev. B **59**, 1758 (1999).
[30] J. P. Perdew, K. Burke, and M. Ernzerhof, Phys. Rev. Lett. **77**, 3865 (1996).
[31] H. J. Monkhorst and J. D. Pack, Phys. Rev. B **13**, 5188 (1976).
[32] P. Souvatzis, O. Eriksson, M. I. Katsnelson, and S. P. Rudin, Comput. Mater. Sci. **44**, 888 (2009).
[33] R. Martoňák, D. Donadio, A. R. Oganov, and M. Parrinello, Nature Mater. **5**, 623 (2006).
[34] Y. Wang, L. G. Hector, Jr., H. Zhang, S. L. Shang, L. Q. Chen, and Z. K. Liu, Phys. Rev. B **78**, 104113 (2008).
[35] R. Martoňák, Eur. Phys. J. B **79**, 241 (2011).
[36] M. Born and K. Huang, *Dynamical Theory of Crystal Lattices* (Oxford University Press, New York, 1954).
[37] Y. Le Page and P. Saxe, Phys. Rev. B **65**, 104104 (2002).
[38] Y. Le Page and J. R. Rodgers, J. Appl. Crystallogr. **38**, 697 (2005).
[39] J. Wang, J. Li, S. Yip, S. Phillpot, and D. Wolf, Phys. Rev. B **52**, 12627 (1995).
[40] L. G. Hector, Jr. and J. F. Herbst, J. Phys.: Condens. Matter **20**, 064229 (2008).
[41] C. C. Silva, H. W. Leite Alves, L. M. R. Scolfaro, and J. R. Leite, Phys. Status Solidi C **2**, 2468 (2005).
[42] P. Pavone, S. Baroni, and S. de Gironcoli, Phys. Rev. B **57**, 10421 (1998).
[43] S. Ganeshan, L. G. Hector, Jr., and Z. K. Liu, Acta Materialia **59**, 3214 (2011).
[44] H. T. Stokes and D. M. Hatch, Phys. Rev. B **65**, 144114 (2002).
[45] A. Polian, M. Grimsditch, and I. Grzegory, J. Appl. Phys. **79**, 3343 (1996).
[46] D. M. Clatterbuck, C. R. Krenn, M. L. Cohen, and J. W. Morris, Jr., Phys. Rev. Lett. **91**, 135501 (2003).
[47] W. Zhou, Y. Zhang, H. Sun, and C. Chen, Phys. Rev. B **86**, 054118 (2012).
[48] M. Parrinello and A. Rahman, J. Appl. Phys. **52**, 7182 (1981).
[49] M. P. Halsall, P. Harmer, P. J. Parbrook, and S. J. Henley, Phys. Rev. B **69**, 235207 (2004).
[50] C.-Y. Yeh, S.-H. Wei, and A. Zunger, Phys. Rev. B **50**, 2715 (1994).